OMTM, Volume *6*

Supplemental Information

Lentiviral Fluorescent Genetic Barcoding for Multiplex Fate Tracking of Leukemic Cells

Tobias Maetzig, Jens Ruschmann, Lea Sanchez Milde, Courteney K. Lai, Niklas von Krosigk, and R. Keith Humphries

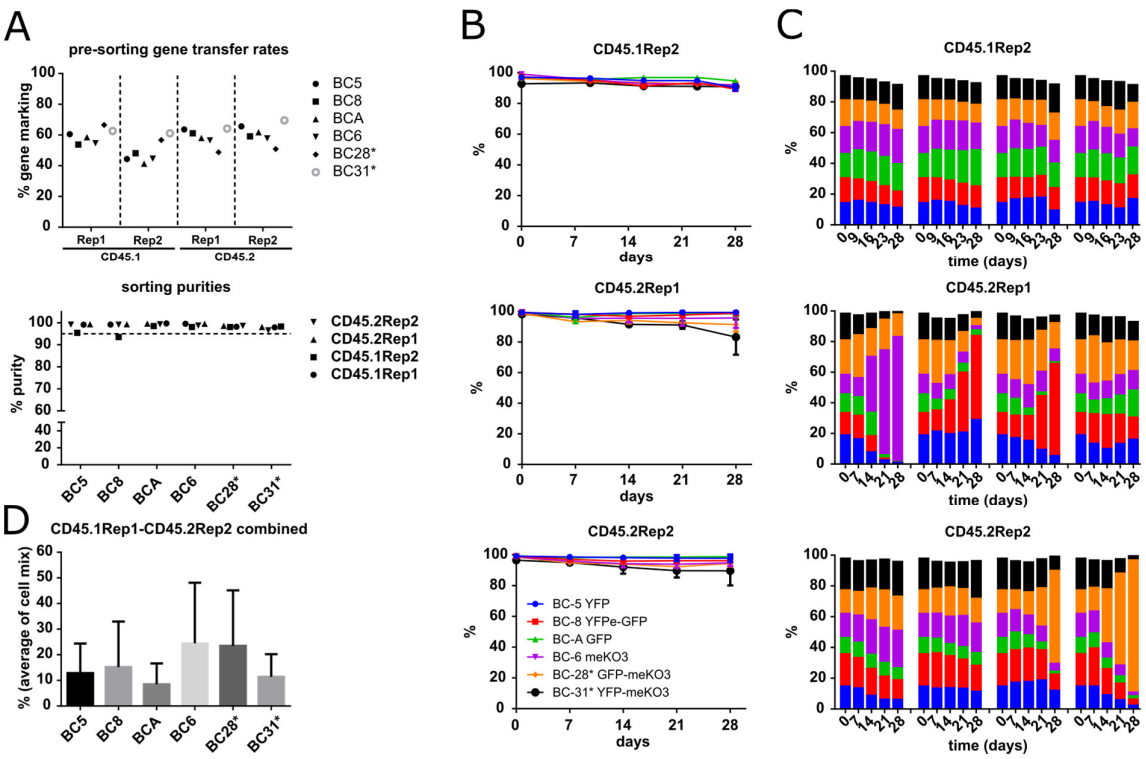

Figure S1: ***In vitro*** **characterization of FGB vector-transduced H9M cells.** (**A**) H9M cells derived from CD45.1Rep1, CD45.1Rep2, CD45.2Rep1 and CD45.2Rep2 lines were transduced with FGB vectors and assessed for (upper graph) gene marking rates in bulk cultures at time of sorting as well as for (lower graph) sorting purities for BCA, BC5, BC6, BC8, BC28* and BC31* color codes by flow cytometry at start of *in vitro* tracking experiments. (**B**) Single purified color-coded H9M populations were tracked over time. One sorted sample was split into four wells for longitudinal analysis, and at least three of those aliquots were tracked for 28 days of observation. Data points indicate mean values ±SD. (**C**) Longitudinal tracking of 6xFGB H9M cell mixes. For (**B**) and (**C**), the day 0 sample is identical for all replicates of a parental H9M line. (**D**) The average contribution of each color-coded population to endpoint total cell mixes from Figures 1G and S1C was plotted. Significant differences between the growth properties of the six color codes could not be detected when using ordinary One-Way ANOVA with post-hoc Turkey multiple comparison testing.

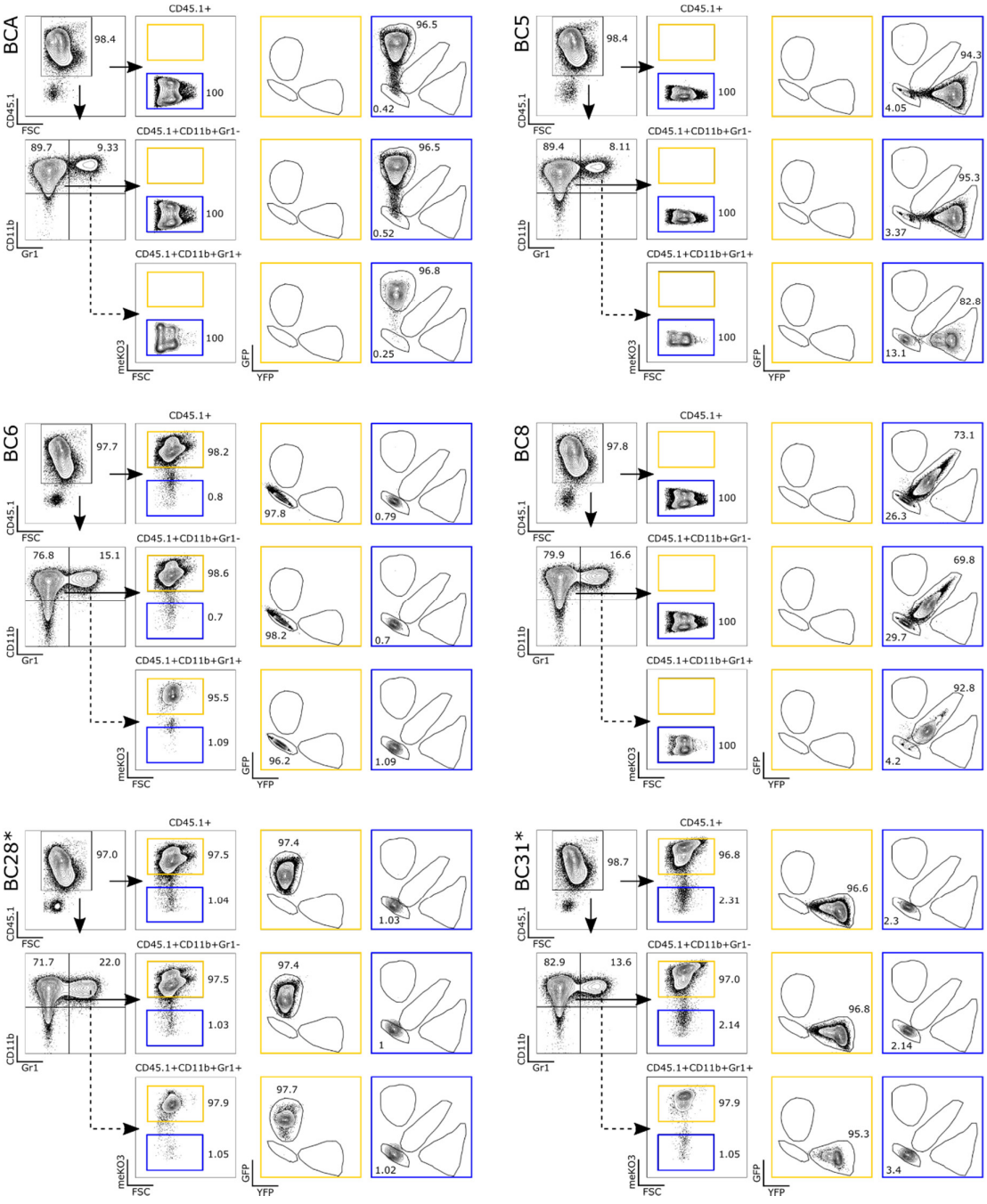

Figure S2: Exemplified phenotypic analysis of PB samples from mice transplanted with single color-coded H9M populations. PB samples stained for CD45.1 donor-derived cells, as well as for CD11b and Gr1 myeloid markers were analyzed by flow cytometry. Within the respective gates, cells were first gated for meKO3 expression prior to plotting GFP vs YFP signals. The percentages within plots with lineage markers refer to the size distribution within the individual plots, whereas color code distributions have been normalized for the parental lineage.

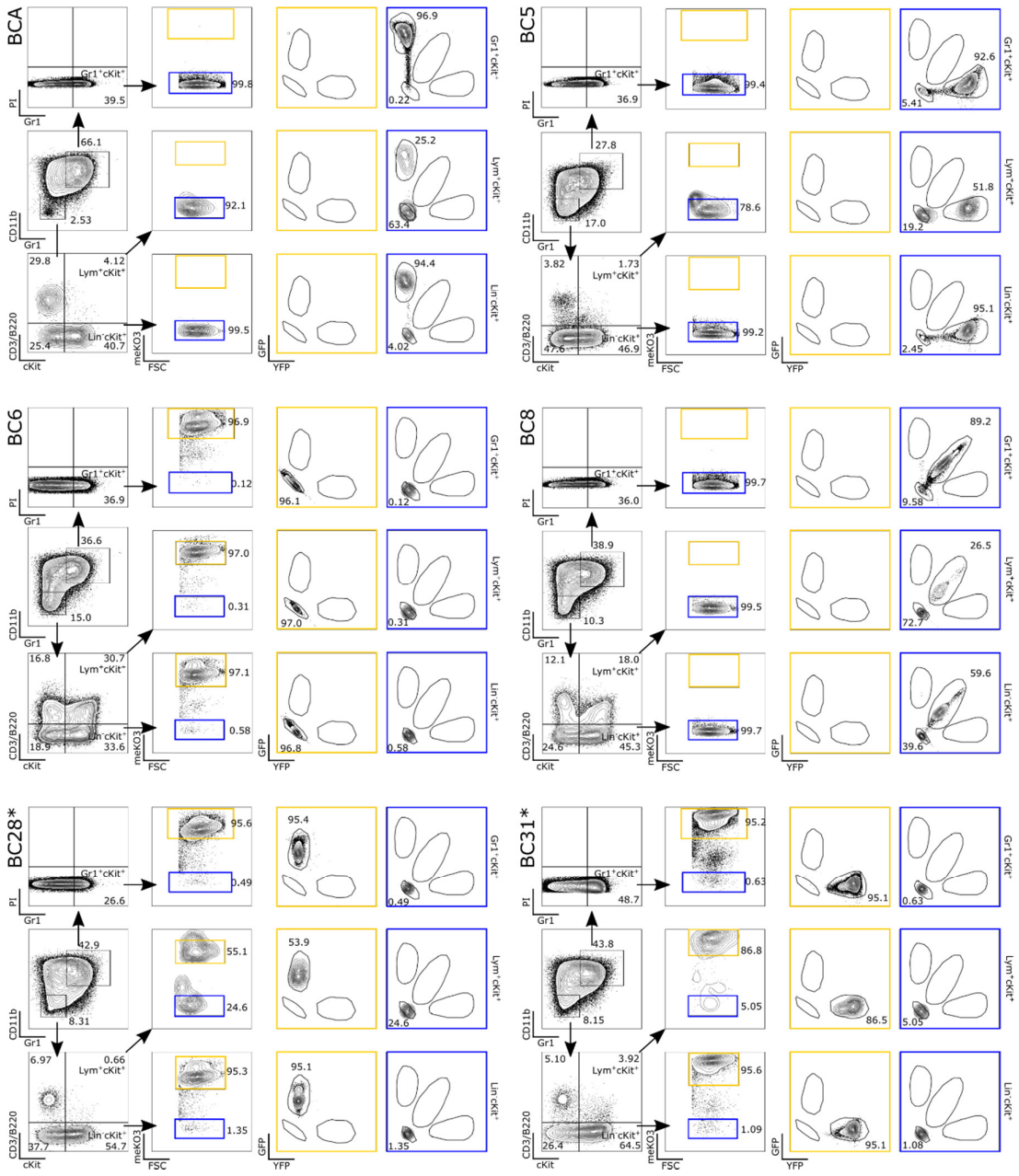

Figure S3: Exemplified phenotypic analysis of BM samples from mice transplanted with single color-coded H9M populations. BM samples of mice shown in Figure S2 were analyzed for color code expression in presumptive LSC subpopulations. First, cells were gated on the presence or absence of myeloid markers CD11b and Gr1. The $Gr1^+cKit^+$ LSC population was then identified in the $CD11b^+Gr1^+$ gate. Myeloid marker negative cells were analyzed for the expression of CD3 and B220 lymphoid (Lym) markers to identify the Lym^+cKit^+ and lineage negative (Lin^-) Lin^-cKit^+ LSC subpopulations, respectively. The percentages within plots with lineage markers refer to the size distribution within the individual plots, whereas color code distributions have been normalized for the parental lineage.

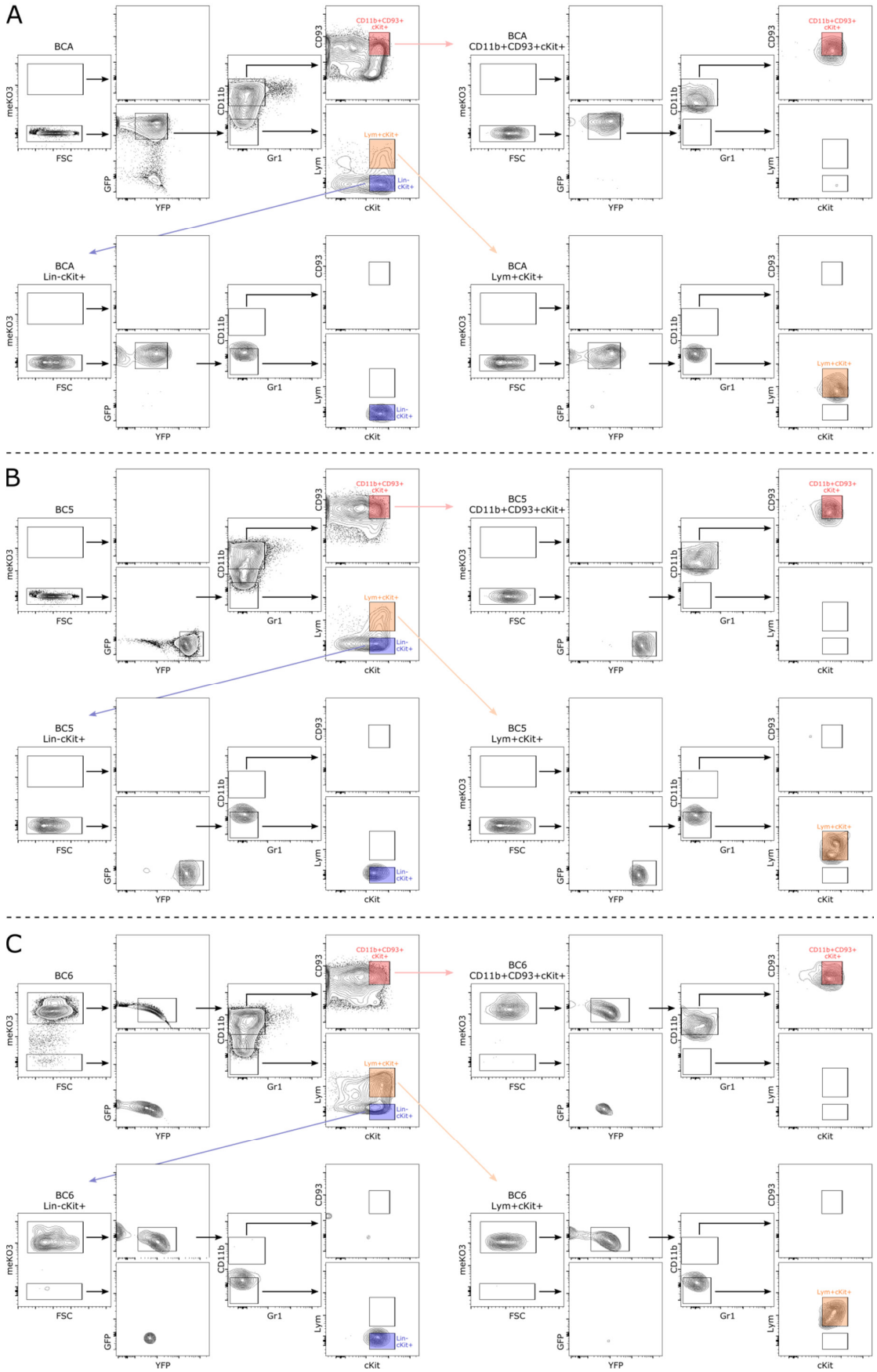
A
BCA
meKO3
FSC
GFP
YFP
CD11b
Gr1
CD93
CD11b+CD93+
cKit+
Lym
Lym+cKit+
Lin-
cKit+
cKit
BCA
CD11b+CD93+cKit+
BCA
Lin-cKit+
BCA
Lym+cKit+
B
BC5
BC5
CD11b+CD93+cKit+
BC5
Lin-cKit+
BC5
Lym+cKit+
C
BC6
BC6
CD11b+CD93+cKit+
BC6
Lin-cKit+
BC6
Lym+cKit+

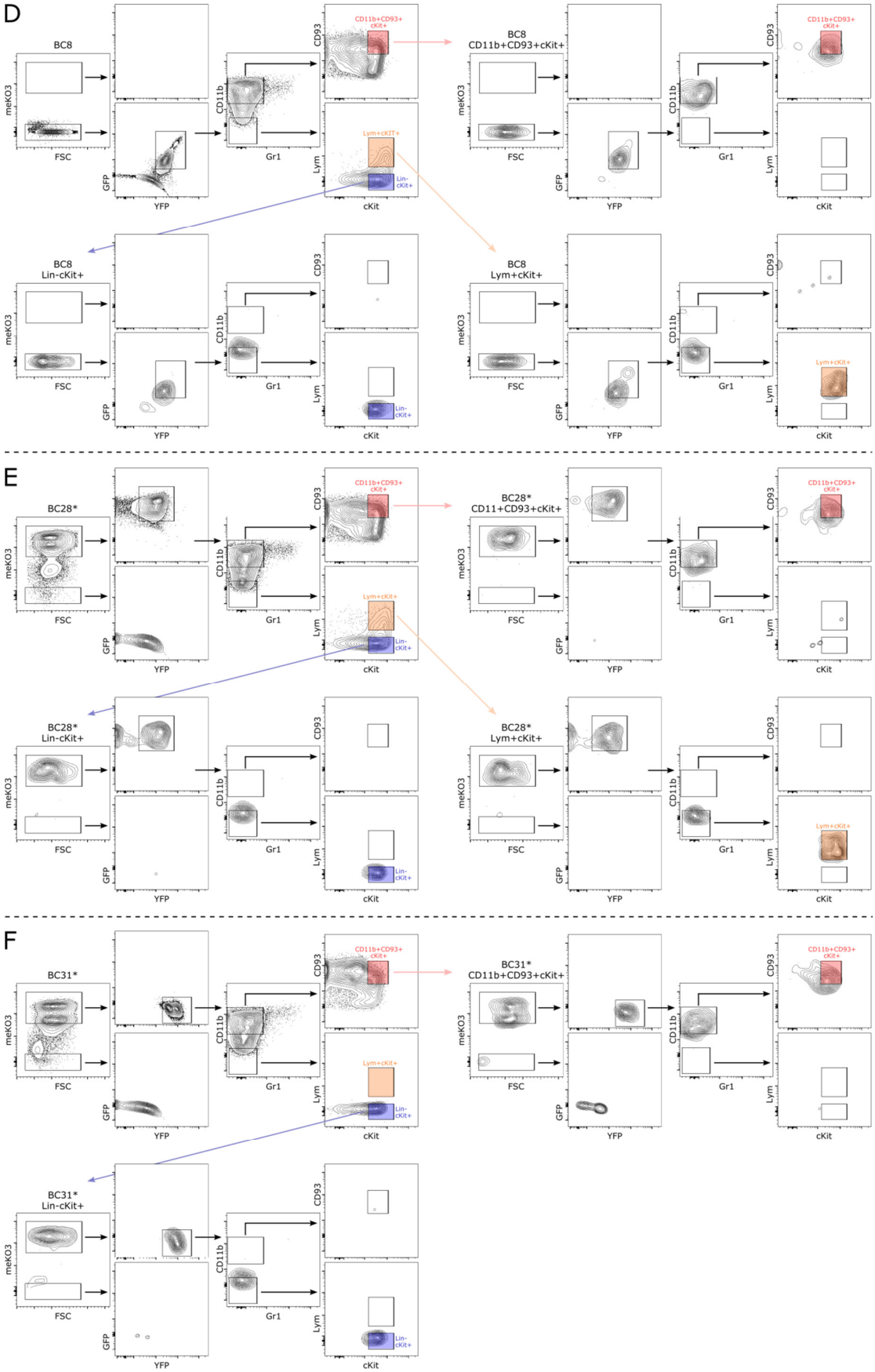
D
BC8
meKO3
FSC
GFP
YFP
CD11b
Gr1
CD93
CD11b+CD93+
cKit+
Lym
Lym+cKIT+
Lin-
cKit+
cKit
BC8
CD11b+CD93+cKit+
BC8
Lin-cKit+
BC8
Lym+cKit+
Lym+cKit+
E
BC28*
BC28*
CD11+CD93+cKit+
BC28*
Lin-cKit+
BC28*
Lym+cKit+
F
BC31*
BC31*
CD11b+CD93+cKit+
BC31*
Lin-cKit+

Figure S4: Sorting strategy for color-coded BM populations with LSC potential. BM cells of mice transplanted with single color-coded H9M cells were stained for CD11b, Gr1, cKit, CD93 and lymphoid markers (Lym; CD3 and B220) prior to sorting of color-coded BM populations with LSC potential. (**A-F**) Upper left plots represent the unfractionated BM samples with sorting gates indicated in red ($CD11b^{+}CD93^{+}cKit^{+}$), orange ($Lym^{+}cKit^{+}$) and blue ($Lin^{-}cKit^{+}$), respectively. The remaining plots show the sorted populations for (**A**) BCA, (**B**) BC5, (**C**) BC6, (**D**) BC8, (**E**) BC28* and (**F**) BC31*. According to Iwasaki *et al* (Cell Stem Cell. 2015), a subset of AML requires CD93 for leukemogenicity.

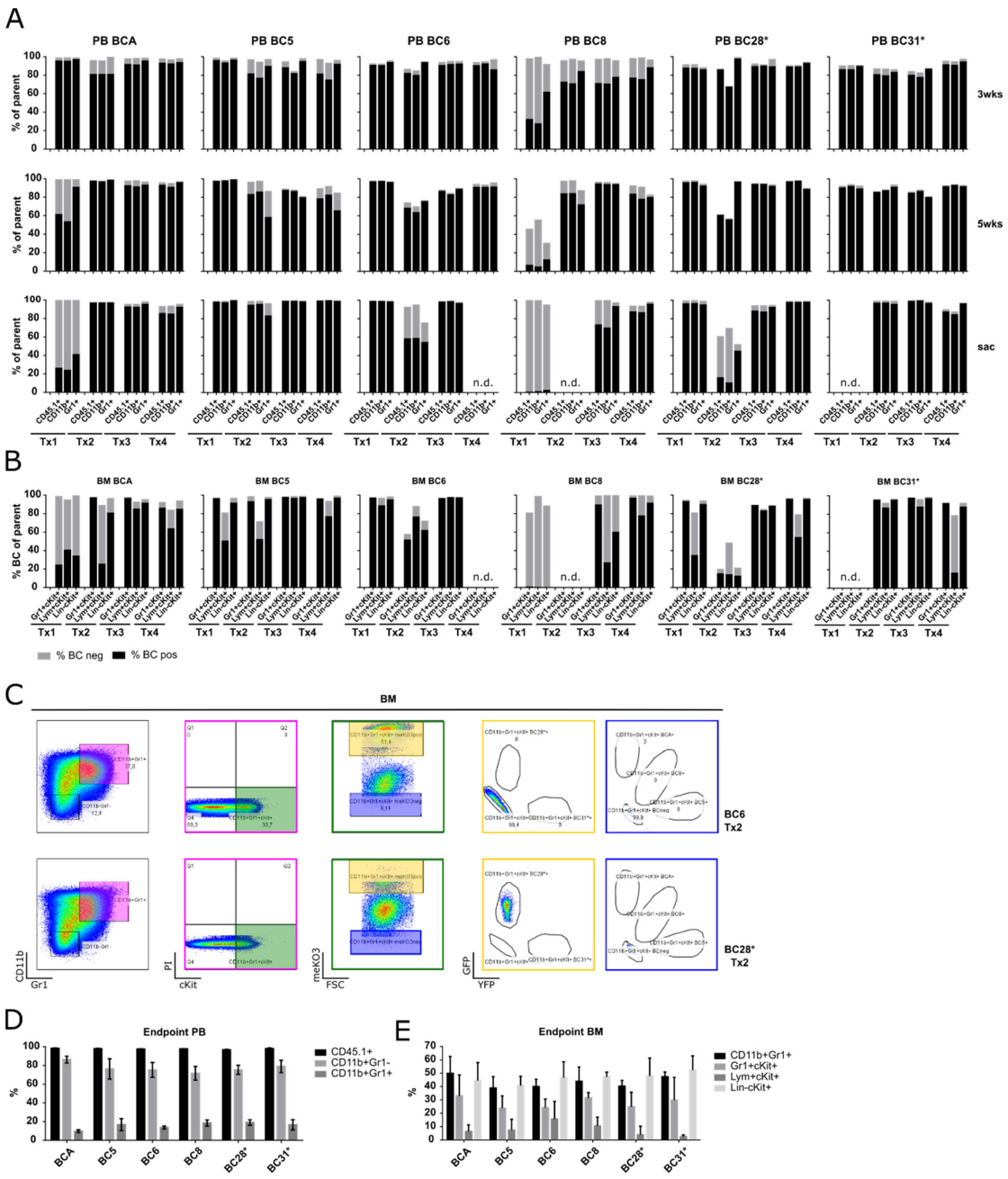

Figure S5: Longitudinal color code distribution in single color code transplanted mice. (**A**) PB analysis of individual mice (Tx1-Tx4) transplanted with single color-coded H9M cells over time. The distribution of CD45.1$^+$, CD45.1$^+$CD11b$^+$Gr1$^-$ (CD11b$^+$) and CD45.1$^+$CD11b$^+$Gr1$^+$ (Gr1$^+$) color-coded cells is shown. (**B**) Analysis of color code distribution of mice from A in BM LSC subpopulations. (**C**) Exemplified BM analysis of mice BC6 Tx2 and BC28* Tx2, which developed an intermediate bright meKO3$^+$ population that was excluded from analyses. (**D,E**) Lineage distribution within color-coded mice at time of sacrifice in (**D**) PB and (**E**) BM.

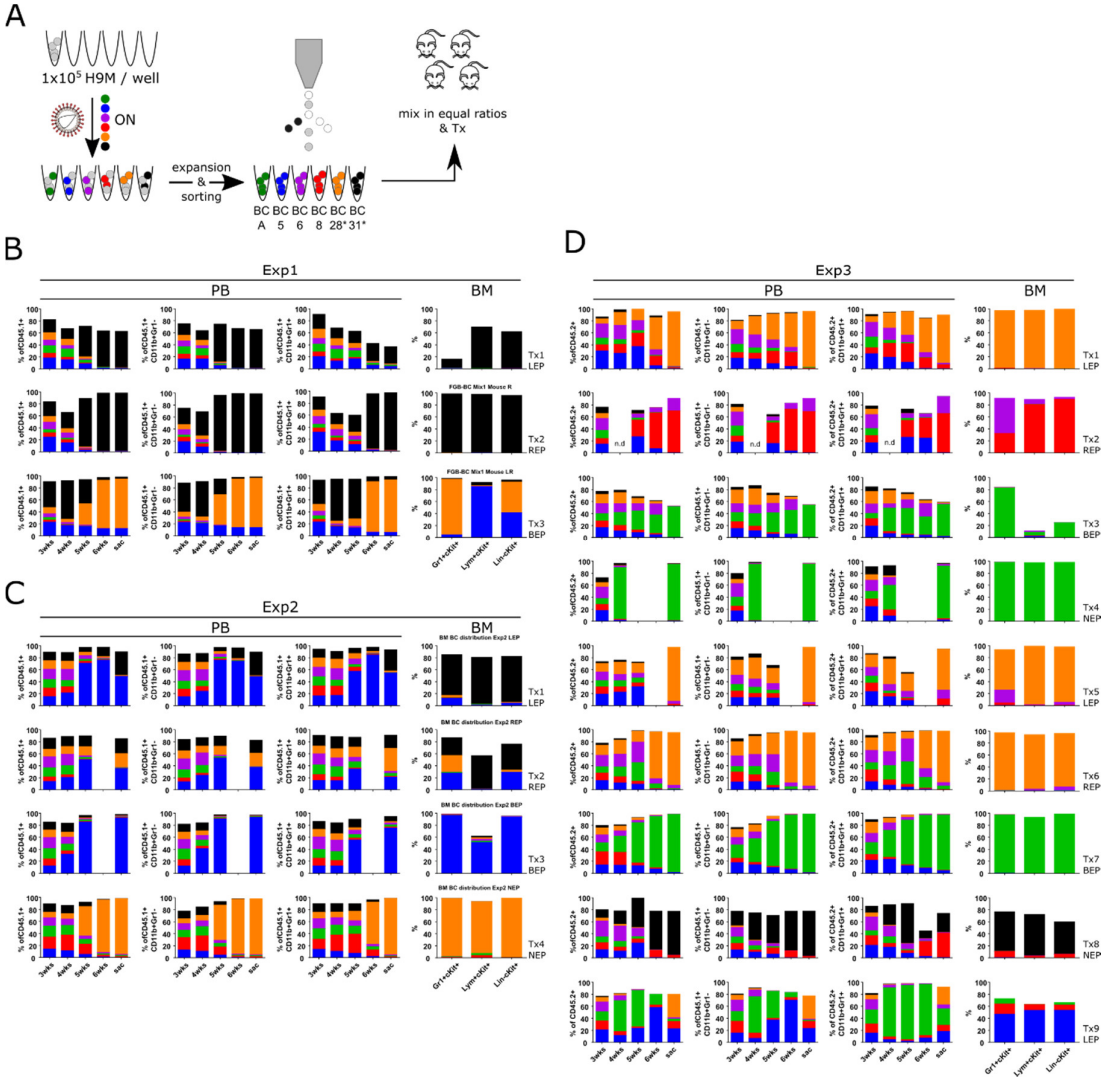

Figure S6: Summary of color code distribution in mice transplanted with 6xFGB H9M cell mixes from three experiments. (**A**) Experimental design. (**B-D**) Figure panels show the color code distribution within PB and BM of mice transplanted in three separate experiments (Exp1-Exp3).

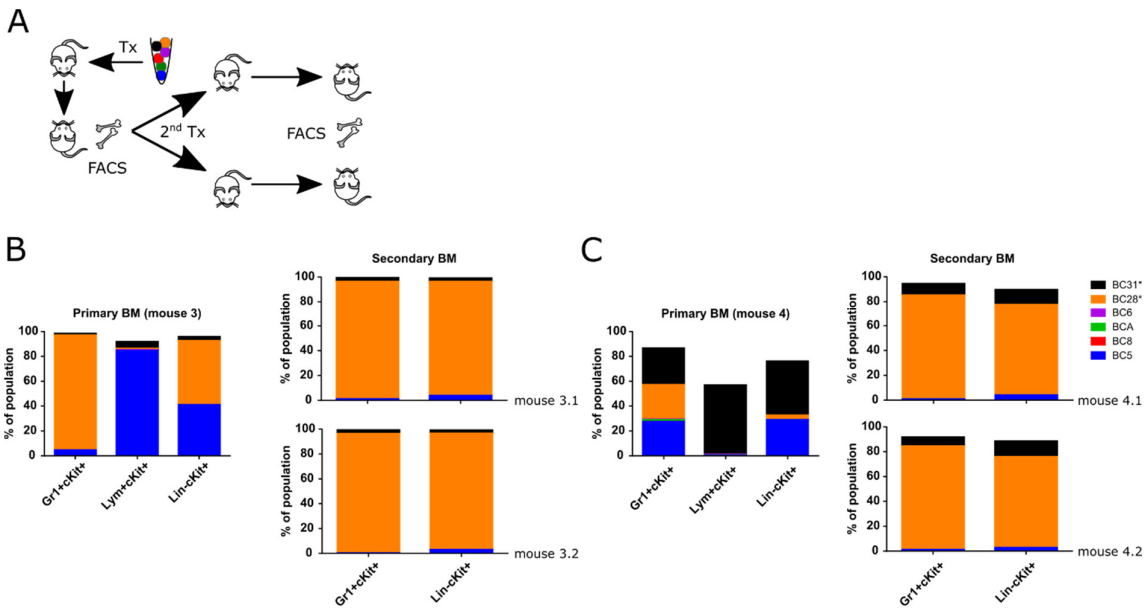

Figure S7: Paired daughter secondary transplantations reveal identical color codes. (**A**) Experimental design. BM of moribund mice was transplanted into two recipients, and color code distributions were determined in BM samples of moribund mice. (**B,C**) Color code distribution in LSC subpopulations of the donor mouse 3 and mouse 4 from Figure 3B as well as in both secondary recipients of each arm.

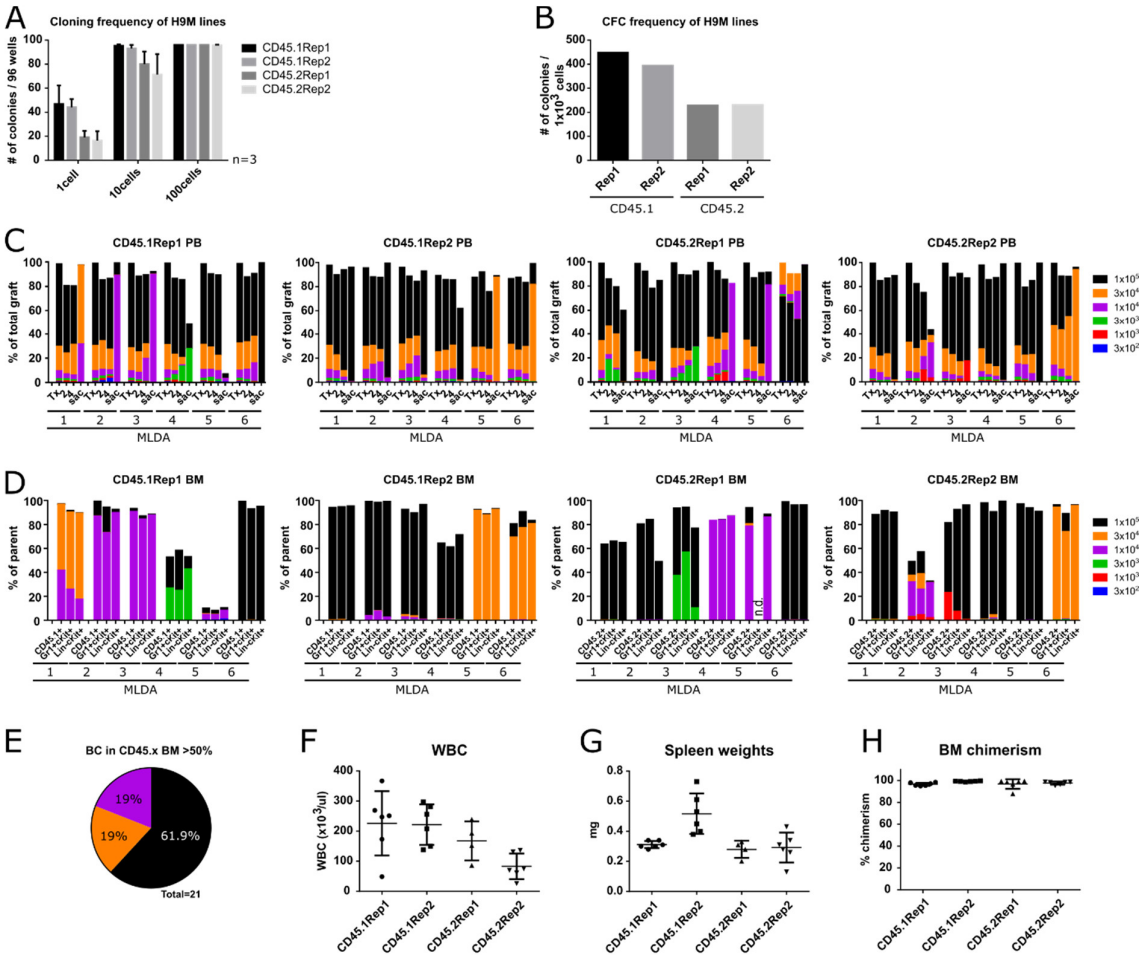

Figure S8: Color code distribution in PB and BM samples of H9M mice from MLDA experiments. (**A**) Determination of the cloning frequency of four individually generated H9M lines. 1, 10 or 100 cells were sorted into 96 well plates and the number of emerging colonies was determined seven days later and normalized to 96 wells. Bar graphs show mean values ±SD from three independent experiments. (**B**) Colony counts of four H9M lines subjected to duplicate colony forming cell assays. Bar graphs show mean values from both plates. (**C**) Analysis of color code distribution in bulk donor-derived PB samples at time of transplantation (Tx; input cell mix), 2 and 4 weeks after transplantation as well as at time of sacrifice (sac). (**D**) Color code distribution in BM subpopulations of moribund mice. (**E**) Dominant (>50% graft contribution) color code distribution in donor-derived BM cells in moribund mice. (**F**) White blood counts, (**G**) spleen weights and (**H**) BM chimerism of moribund mice. Error bars in F-H indicate mean values ±SD.

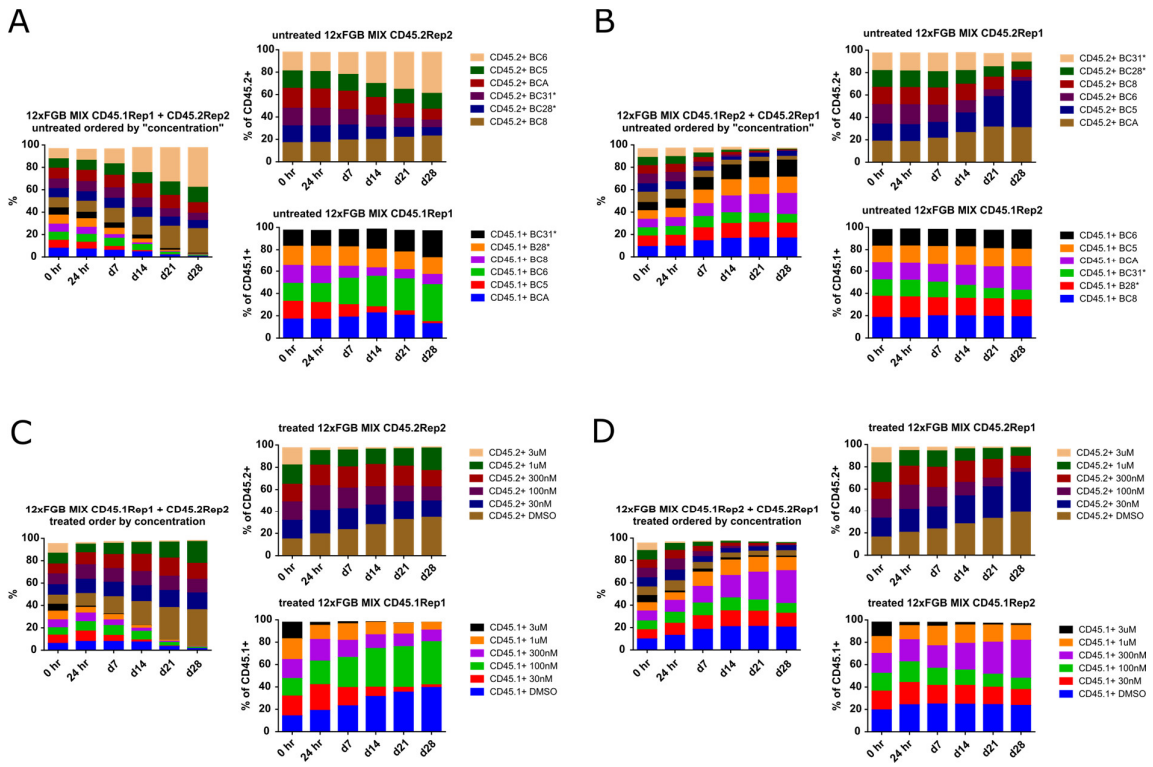

Figure S9: Longitudinal tracking of 12xFGB H9M cell mixes. Untreated or 24 hr Entinostat-exposed color-coded CD45.1- and CD45.2-derived H9M cells were mixed in equal ratios and tracked over time (0 hr = starting cell mix; and after 24 hr, 7, 14, 21 and 28 days, respectively). (**A**) Left panel: tracking of untreated CD45.1Rep1 and CD45.2Rep2 color-coded 12xFGB cell mix over time. The cell mix was stained with CD45.1 and CD45.2 antibodies, and the contribution of color-coded populations within the CD45.1 and CD45.2 gates was expressed as a fraction of the total viable (PI neg.) cells. Right panels: Color codes from the 12xFGB cell mix were expressed as a fraction of the parental $CD45.1^+$ (lower plot) and $CD45.2^+$ (upper plot) gates, respectively. This neglects the influence of the H9M line indigenous growth rate on color code distributions from the 12xFGB mix. (**B**) Same as A, but with CD45.1Rep2- and CD45.2Rep1-derived 12xFGB cell mix. (**C**) CD45.1Rep1- and CD45.2Rep2-derived color-coded cells were treated with increasing concentrations of Entinostat for 24hrs. Afterwards, cells were washed and mixed in equal ratios. Left panel: Color code contributions to the total cell mix were subsequently assessed over time as in A. Right panels: The 12xFGB mix was analyzed for color code distributions within the CD45.1- (lower panel) and CD45.2- (upper panel) derived populations. (**D**) Same as C, but with CD45.1Rep2- and CD45.2Rep1-derived color-coded cells.